2021 XVIII Congreso Internacional de Ingeniería Eléctrica, Ciencias de la Computación y Control Automático (CCE). Ciudad de México, México. 10-12 de noviembre de 2021

Improving thermal stability of perovskite solar cell through interface modification by PbS quantum dots

Evelyn B. Díaz-Cruz
Facultad de Química. UAQ
Santiago de Querétaro, Qro, México
ebdc@ier.unam.mx

E. Regalado-Pérez
Instituto de Energías Renovables. UNAM
Temixco, Morelos, México
eurepe@ier.unam.mx

Jorge Cruz-Gómez
Facultad de Química. UAQ
Santiago de Querétaro, Qro, México
jorge_jcg@icloud.com

X. Mathew
Instituto de Energías Renovables. UNAM
Temixco, Morelos, México
xm@ier

F. J. de Moure-Flores
Facultad de Química. UAQ
Santiago de Querétaro, Qro, México
fcomoure@hotmail.com

Francisco Paraguay-Delgado
Centro de Investigación en Materiales Avanzados
Chihuahua, Chih México
francisco.paraguay@cimav.edu.mx

Jose Santos-Cruz
Facultad de Química. UAQ
Santiago de Querétaro, Qro, México
jsantos@uaq.edu.mx

***Abstract*— Colloidal quantum dots (QDs) are widely utilized for the development of light-emitting diodes (LEDs), photodetectors, and solar cells. Herein, PbS QDs were incorporated as interfacial modifiers between the perovskite layer and the hole-transporting material (HTM) in perovskite solar cells (PSCs). The results reveal that the use of PbS QDs leads to improved device thermal stability. This work proposes a method for analyzing the thermal stability of PSCs based on the impedance spectroscopy technique.**

Keywords*— *perovskite solar cell, PbS quantum dots, thermal stability

I. INTRODUCTION

While organic-inorganic hybrid perovskite solar cells have made significant progress in terms of power conversion efficiency over the last decade, the severe instability of these devices under real operational conditions is the major challenge for commercialization [1]. It is well known that metal halide perovskite solar cells can degrade when exposed to moisture, oxygen, heat, light, mechanical stress, and reverse bias [2]. It has been reported that methylammonium lead iodide (MAPI) decomposes slowly at 65 to 85°C, which is the temperature at which solar panels are typically exposed under environmental conditions, and decomposes rapidly at 135 to150 °C, which is the temperature at which encapsulated solar cells are tested [3], [4]. This decomposition has been related to a tetragonal-to-cubic phase transition in perovskite [5], which can occur rapidly at 100°C [6], [7]. On the other hand, inhibiting the mobilization of iodide ions may be able to prevent these phase changes. In general, increasing PSC stability requires a deeper understanding of how perovskite devices degrade under various environments. Electrochemical Impedance Spectroscopy (EIS) is a very effective technique for analyzing charge transfer and transport processes in solar cells. In particular, EIS analysis of PSCs has revealed a wide range of behaviours [8].

In this work, the thermal stability of PSCs with and without PbS quantum dots as an interfacial layer between perovskite film and spiro-MeOTAD is investigated using EIS. The results reveal that the PbS QDs maintain and even decrease the charge extraction resistance when the device is heated at 100°C.

FONDEC-UAQ-2021

II. EXPERIMENTAL PROCEDURE

A. PbS quantum dots preparation

The following reagents were utilized in the synthesis of PbS QDs: Lead oxide (PbO), Meyer (purity of 99%); oleic acid ($C_{18}H_{34}O_2$) (OA), Meyer (reactive grade); bis(trimethyl silyl) sulfide ($(CH_3)_3SiSSi(CH_3)_3$) (TMS), Beantown Chemical (purity 98%); 1-octadecene ($CH3(CH_2)_{15}CH=CH$) (ODE), GFS Chemicals (purity 90%); 1.2 ethanedithiol $HSCH_2CH_2SH$ (EDT), Sigma-Aldrich (purity of 98%); methanol, acetone, toluene, and chlorobenzene (CB) as solvents. All materials were used as received. The PbS QDs were obtained following the procedure reported by Hines and Scholes [9], with some modifications. In brief, the reaction was conducted in a three-

978-1-6654-0029-9/21/$31.00 ©2021 IEEE

mouthed flask under a nitrogen atmosphere. The lead precursor was obtained by mixing PbO with OA and ODE in the flask and stirring for one hour at 150 °C. The sulphur precursor was obtained by mixing the TMS with ODE. The temperature of the solution was then adjusted with the lead precursor to the temperature at which the synthesis was carried out (140 °C), and the sulphur precursor solution was afterwards injected. It was kept at that temperature for 5 minutes and then cooled rapidly to 40°C. Subsequently, methanol and acetone were added, and the nitrogen atmosphere was removed. Finally, the obtained PbS QDs were collected by centrifugation, washed successively with methanol, acetone, and toluene, respectively, and dried in vacuum for 24 h. The PbS QDs were dispersed in toluene for further use. To use QDs in solar cells, a different binder must be used [10][11]; i.e., oleic acid must be replaced with a binder with superior electrical properties. EDT was employed in this case. EDT was added to the PbS QD solution in toluene at a 4:1 (toluene:EDT) volume ratio for the ligand change, and the mixture was stirred at 70°C for 12 hours in an oil bath. It was then left to stir at room temperature for another 24 hours. Afterwards, the samples were washed successively with methanol, acetone, and toluene using centrifugation. Lastly, the dry material was dissolved at a concentration of 25 mg/mL in a 9:1 mixture of CB:EDT.

B. Device fabrication

Fluorine-doped tin oxide (FTO) glass substrates were patterned by etching with Zn powder and 1 M HCl diluted in deionized (DI) water. The patterned FTO substrates were cleaned with neutral detergent, DI water, acetone and isopropanol in an ultrasonic bath for 10 min each, followed by an additional cleaning step in an oxygen plasma for 15 min immediately before the deposition of the charge transport layer. A compact SnO_2 layer was developed as an electron transport layer (ETL) via chemical bath deposition (CBD). In brief, 500 mg urea was dissolved in DI water, followed by the addition of 10 µL thioglycolic acid and 0.5 mL HCl (37 wt%). After that, 0.1g $SnCl_2 \cdot 2H_2O$ was added to the solution, which was stirred for 5 min. The FTO substrates were immersed into the aforementioned solution for 4 h at 80 °C with magnetic agitation, then washed in DI water and dried under a nitrogen stream. Finally, the films were annealed at 200 °C for 30 min in a muffle furnace under ambient air. The SnO_2 substrates were treated with oxygen plasma for 15 min before being transferred into the N_2-filled glove box for perovskite deposition. The perovskite precursor solution was prepared using mixed-cation lead mixed-halide perovskite with the nominal formula $[FAPbI_3]_{83}[MAPbBr_3]_{17}$. To form $FAPbI_3$ and $MAPbBr_3$ precursor solutions, FAI and PbI_2 or MABr and $PbBr_2$ were dissolved in DMF/DMSO (4:1 v/v%) in a 1:1.09 molar ratio, according to previously reported procedure [12]. The final perovskite solution was prepared by mixing the precursor solutions of $FAPbI_3$ and $MAPbBr_3$ in a 5:1 v/v ratio. The perovskite layers were deposited by a one-step spin-coating at 3500 rpm for 30 s, and 10 s prior to the end, 150 µL of green antisolvent ethyl acetate (EA) was dropped onto the substrate. After that, the sample was annealed on a hot plate at 100°C for 30 min. PbS QDs QDs at a concentration of 2 mg/ml were dynamically spin-coated on perovskite film at 2000 rpm for 30 seconds, followed by heating at 100 °C for 2 min.

Hole transport layer (HTL) was then deposited via spin-coating a 70 mM solution of Spiro-MeOTAD in chlorobenzene, with additives of Li-TFSI, 4-tert-butylpyridine (t-BP) and FK269. Spin-coating was carried out at 3000 rpm for 30 s. Finally, the devices were completed by thermal evaporation of 80 nm of Au as the top electrode with an active area equal to 0.1 cm^2. The final devices are shown in Fig.1a&b.

C. Characterization

EIS measurements were carried out under AM1.5 illumination and with different forward biases using a VSP potentiostat (Biologic Science Instruments). The device temperature was increased from 38°C to 100°C while the EIS data was taken at the same time. The equivalent circuit of Fig.2f was used to fit the experimental EIS data using the *Z* fit tool in EC-Lab Software. HRTEM images were taken with a Nanotech TEM JEOL 2200FS+CS. The samples were prepared by drop-casting of diluted perovskite with PbS QDs ink onto an ultrathin carbon 3 mm grid and allowed to slowly dry to 60°C. The current density-voltage (J-V) characteristics of perovskite devices were measured under AM1.5G illumination from a solar simulator (Sol3A Class AAA, Oriel Instruments). The incident light power was adjusted to 1000 W/m^2 using a calibrated Si reference cell supplied by Newport (91150V).

III. RESULTS AND DISCUSSION

The architecture of the two types of perovskite devices explored here is shown in Fig. 1: a) reference device, and b)

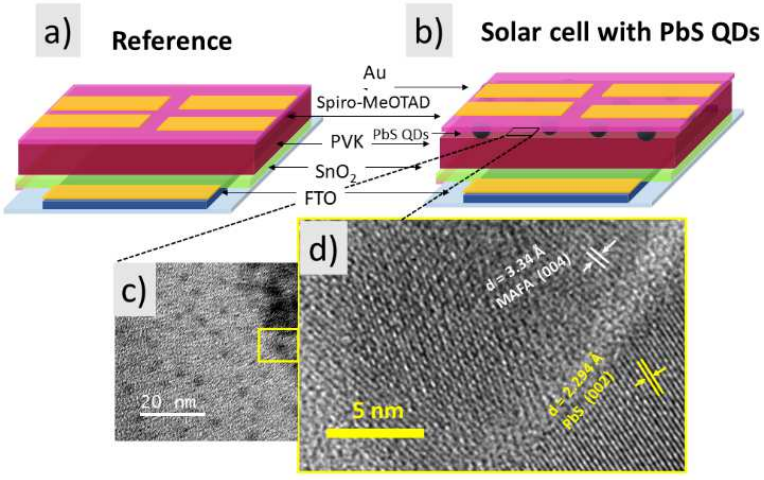

Fig.1 Schematic illustration of the device architecture used for PSC fabrication: a) Reference device (without PbS QDs) and b) device with interfacial layer of PbS QDs incorporated between the perovskite layer and the spiro-MeOTAD, c) HRTEM image of perovskite/PbS QDs and d) the lattice spacing for PbS QDs (2.29Å); and perovskite (3.34 Å).

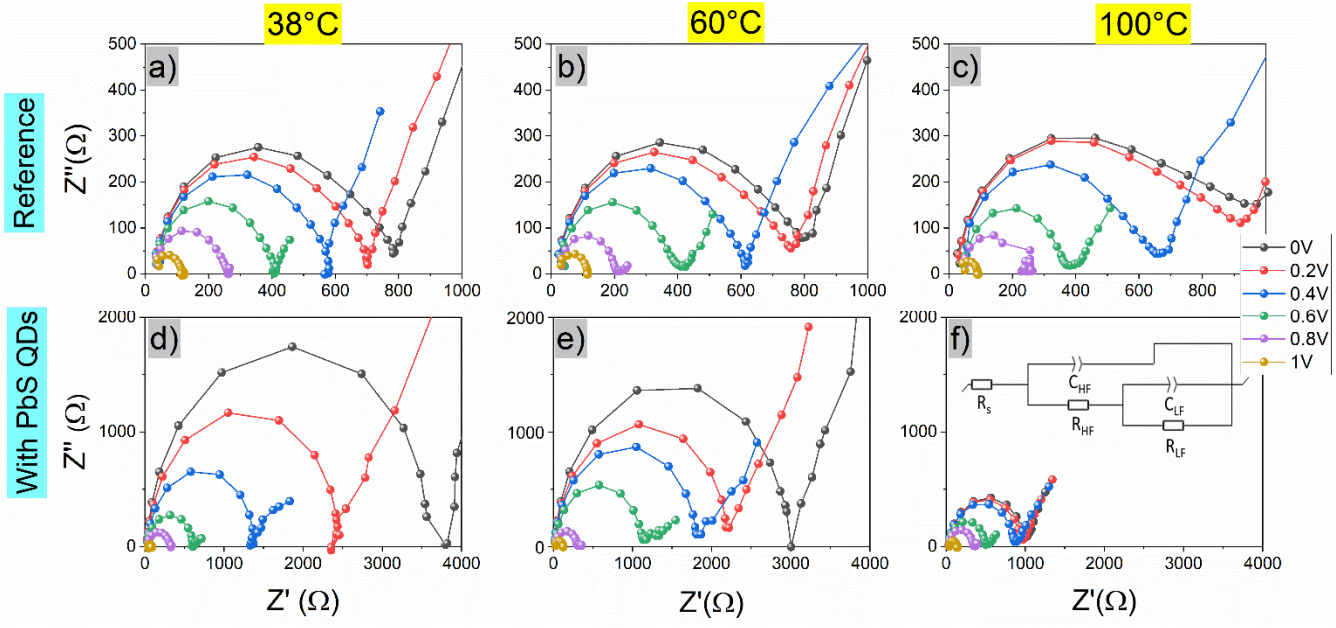

Fig.2 EIS Nyquist plots measured at different temperatures for PSCs: a), b) & c) without PbS QDs and d), e) & f) with interfacial layer of PbS QDs.

device with a PbS QDs interfacial layer between the HTL and the perovskite layer.

HRTEM images of perovskite/PbS QD samples were obtained to visualize the perovskite matrix with embedded QDs. The PbS QDs on perovskite material with sizes ranging from 5 to 10 nm are shown in Fig.1c, while the lattice spacings of both cubic PbS and perovskite (MAFA) can be seen in Fig.1d, along with their relative orientations, indexed to the planes (002) and (004), respectively[14], [15]. The Nyquist plots (Fig. 2) show two arcs in both cases, which can be represented by RC elements in an equivalent circuit. In light of this, the circuit depicted in the inset of Fig.2f was used to obtain a good fit, where Rs is the series resistance related to the contact resistance and the FTO resistance, R_{HF} resistance and C_{HF} capacitance describe high-frequency behaviour, while R_{LF} and C_{LF} elements correlate to low-frequency components. A constant phase element was used instead of an ideal capacitor to model the spatial inhomogeneity induced by defects and impurities at the interfaces [16]. As can be seen in Fig. 2a-c, the first arc for the reference device is smaller at low voltages (<0.4 V), indicating a lower R_{HF} and improved charge extraction [17]. However, when the temperature increases it is observed that the size of the arc increases, and consequently an increase in the charge extraction resistance is reached. However, as the temperature rises, the size of the first arc increases due to increased charge extraction resistance.

Although the arcs in the device with PbS QDs are greater at 38 ° C and 60 ° C than in the reference device, when the device is heated to 100 ° C, the arc diameters in the device with PbS QDs are smaller than in the reference device, indicating a lower charge extraction resistance, and consequently a more efficient and stable charge carrier collection. Figure 3 shows the fitting parameters extracted from EIS data. The device with PbS QDs exhibits a lower high-frequency resistance (R_{HF}) as the temperature rises (blue line in Fig.3a), whereas the reference device presents an increasing R_{HF} as the temperature increases (red line in Fig.3a). Similar

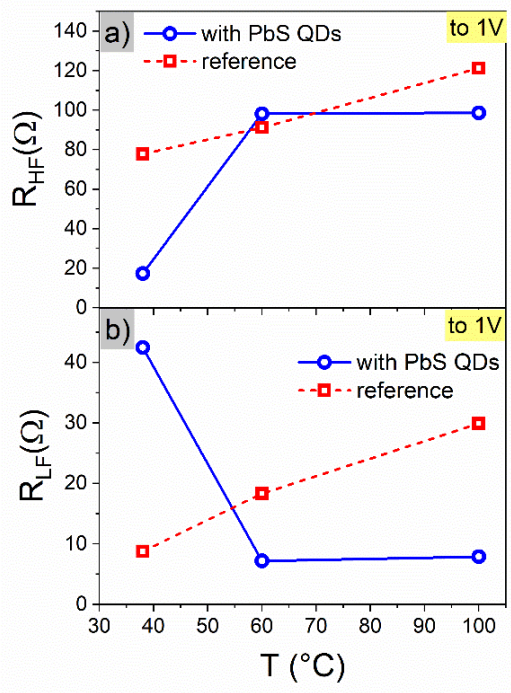

Fig.3 a) The high-frequency resistance (R_{HF}), and b) the low-frequency resistance (R_{LF}) for devices with and without PbS QDs, as a function of temperature, measured at a forward bias of 1V.

behaviour has been reported previously [8]. Likewise, the low-frequency resistance (R_{LF}) in a device using PbS QDs reduces as the temperature rises (Fig.3b). The above suggests that the reference device (without PbS QDs) degrades when exposed to temperatures beyond 100°C. In general, ion migration in halide perovskite films causes device degradation [7], [18]–[20], At high temperatures (85 °C), I^- and MA^+ ions can diffuse into the spiro-OMeTAD layer in the form of CH_3NH_3I (MAI). The diffused I^- ions prevent oxidation of spiro-OMeTAD, diminishing its electrical characteristics [21].

Therefore, we propose that the interfacial layer of PbS QDs incorporated between the perovskite layer and the spiro-MeOTAD acts as a diffusion barrier for ions, as well as for the charge extraction. This explains why the R_{HF} in devices with PbS QDs is higher at low temperatures (38 °C) but lower at higher temperatures (100 °C), where the degradation is more drastic due to accelerated ion migration [7]. As a result, the device containing the PbS QDs retains ion migration, which is seen as a significant reduction in R_{HF} as shown in Fig. 3 a&b, and thus the effect of the PbS QDs interfacial layer can contribute to maintaining the thermal stability of perovskite solar cells.

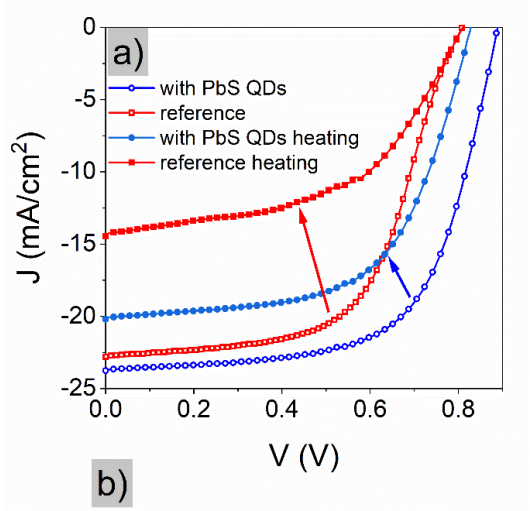

Condition	V_{oc}	J_{sc}	FF	PCE (%)
With PbS	0.88	23.69	63.69	13.42
PbS – heating	0.83	20.09	60.25	10.03
Reference	0.81	22.75	58.40	10.77
Ref - heating	0.80	14.30	51.69	5.98

Fig.4 a) J-V characteristics of PSCs without and with interfacial layer of PbS QDs, before and after heating to 100°C, and b) J-V parameters of the devices.

Figures 4a&b show the photovoltaic performance of the devices under 1 Sun illumination (AM 1.5G) before and after heating. The results show that the solar cell with PbS QDs outperforms the reference device, especially in terms of open-circuit voltage (Voc), resulting in a maximum power conversion efficiency (PCE) of 13.42%. Previous research in QD films found a similar trend, which was attributed to improved carrier transport and lower sub-bandgap trap-state assisted recombination, resulting in improved charge collection in the device [14], [18], [22]–[25].

In order to monitor the stability of PSCs as the temperature increased, we followed the evolution of the photovoltaic performance after heating to 100°C. According to our findings, the perovskite-PbS QDs solar cell maintained 94.31% of V_{oc}, 84% of J_{sc}, and 74.7% of PCE. In comparison, the photovoltaic parameters of the reference device decreased to 1.24% of V_{oc}, 37.14% of J_{sc}, and 55.52% of PCE (Fig.3b). As a result, as the temperature rises above 100°C, the performance of the reference device begins to deteriorate more noticeably, which is most likely due to perovskite degradation via ion migration, as evidenced by EIS results.

IV. CONCLUSIONS

This study compared two types of heated PSCs, one without and one with a PbS QDs interfacial layer incorporated between the perovskite film and the spiro-MeOTAD. Based on our findings, we concluded that the interfacial layer of PbS QDs can aid in improving the thermal stability of perovskite solar cells, which can be degraded due to ion migration when exposed to high temperatures. When the PbS QDs layer is incorporated over the perovskite layer, the mobile ions are trapped and prevented from migrating, thus preventing phase transition. This is reflected in the J-V characteristics, which show that after heating to 100 ° C, the device with PbS QDs maintains 74.7% of its PCE, whereas the device without PbS QDs loses more than 50% of its PCE. Although there is still much work to be done with QDs to improve the stability of perovskite solar cells, this research sheds light on their role in preventing thermal degradation.

ACKNOWLEDGEMENT

The authors acknowledge the financial support of FONDEC-UAQ-2021

REFERENCES

[1] H. Zheng *et al.*, "Enhanced Performance and Stability of Perovskite Solar Cells Using NH4I Interfacial Modifier," *ACS Appl. Mater. Interfaces*, vol. 9, no. 46, pp. 41006–41013, Nov. 2017, doi: 10.1021/acsami.7b12721.

[2] C. C. Boyd, R. Cheacharoen, T. Leijtens, and M. D. McGehee, "Understanding Degradation Mechanisms and Improving Stability of Perovskite Photovoltaics," *Chem. Rev.*, vol. 119, no. 5, pp. 3418–3451, Mar. 2019, doi: 10.1021/acs.chemrev.8b00336.

[3] "Halide Engineering for Mitigating Ion Migration and Defect States in Hot-Cast Perovskite Solar Cells | ACS Sustainable Chemistry & Engineering."

https://pubs.acs.org/doi/10.1021/acssuschemeng.1c02537 (accessed Jul. 06, 2021).

[4] K. Cao *et al.*, "Durable Defect Passivation of the Grain Surface in Perovskite Solar Cells with π-Conjugated Sulfamic Acid Additives," *ACS Appl. Mater. Interfaces*, vol. 13, no. 22, pp. 26013–26022, Jun. 2021, doi: 10.1021/acsami.1c04601.

[5] A. Dualeh, P. Gao, S. I. Seok, M. K. Nazeeruddin, and M. Grätzel, "Thermal Behavior of Methylammonium Lead-Trihalide Perovskite Photovoltaic Light Harvesters," *Chem. Mater.*, vol. 26, no. 21, pp. 6160–6164, Nov. 2014, doi: 10.1021/cm502468k.

[6] E. J. Juarez-Perez, Z. Hawash, S. R. Raga, L. K. Ono, and Y. Qi, "Thermal degradation of CH3NH3PbI3 perovskite into NH3 and CH3I gases observed by coupled thermogravimetry–mass spectrometry analysis," *Energy Environ. Sci.*, vol. 9, no. 11, pp. 3406–3410, Nov. 2016, doi: 10.1039/C6EE02016J.

[7] N.-K. Kim *et al.*, "Investigation of Thermally Induced Degradation in CH 3 NH 3 PbI 3 Perovskite Solar Cells using In-situ Synchrotron Radiation Analysis," *Scientific Reports*, vol. 7, no. 1, Art. no. 1, Jul. 2017, doi: 10.1038/s41598-017-04690-w.

[8] L. Contreras-Bernal *et al.*, "Impedance analysis of perovskite solar cells: a case study," *J. Mater. Chem. A*, vol. 7, no. 19, pp. 12191–12200, May 2019, doi: 10.1039/C9TA02808K.

[9] M. A. Hines and G. D. Scholes, "Colloidal PbS Nanocrystals with Size-Tunable Near-Infrared Emission: Observation of Post-Synthesis Self-Narrowing of the Particle Size Distribution," *Advanced Materials*, vol. 15, no. 21, pp. 1844–1849, 2003, doi: 10.1002/adma.200305395.

[10] M. Nam, T. Lee, S. Kim, S. Kim, S. W. Kim, and K. K. Lee, "Two strategies to enhance efficiency of PbS quantum dot solar cells: Removing surface organic ligands and configuring a bilayer heterojunction with a new conjugated polymer," *Organic Electronics*, vol. 15, no. 2, pp. 391–398, 2014, doi: 10.1016/j.orgel.2013.11.041.

[11] X. Yao *et al.*, "Improved stability of depletion heterojunction solar cells employing cation-exchange PbS quantum dots," *Solar Energy Materials and Solar Cells*, vol. 164, no. February, pp. 122–127, 2017, doi: 10.1016/j.solmat.2017.02.006.

[12] M. Saliba, M. Stolterfoht, C. M. Wolff, D. Neher, and A. Abate, "Measuring Aging Stability of Perovskite Solar Cells," *Joule*, vol. 2, no. 6, pp. 1019–1024, Jun. 2018, doi: 10.1016/j.joule.2018.05.005.

[13] M. Saliba *et al.*, "How to Make over 20% Efficient Perovskite Solar Cells in Regular (n–i–p) and Inverted (p–i–n) Architectures," *Chem. Mater.*, vol. 30, no. 13, pp. 4193–4201, Jul. 2018, doi: 10.1021/acs.chemmater.8b00136.

[14] M. Albaladejo-Siguan *et al.*, "Efficient and Stable PbS Quantum Dot Solar Cells by Triple-Cation Perovskite Passivation," *ACS Nano*, vol. 14, no. 1, pp. 384–393, Jan. 2020, doi: 10.1021/acsnano.9b05848.

[15] N. Cho *et al.*, "Pure crystal orientation and anisotropic charge transport in large-area hybrid perovskite films," *Nat Commun*, vol. 7, no. 1, p. 13407, Nov. 2016, doi: 10.1038/ncomms13407.

[16] Z. Zhang *et al.*, "Enhanced performance of planar perovskite solar cells based on low-temperature processed TiO2 electron transport layer modified by Li2SiO3," *Journal of Power Sources*, vol. 392, pp. 1–7, Jul. 2018, doi: 10.1016/j.jpowsour.2018.04.086.

[17] E. Regalado-Pérez, E. B Díaz-Cruz, J. Landa-Bautista, N. R. Mathews, X. Mathew, "Impact of vertical inhomogeneity on the charge extraction in perovskite solar cells: a study by depth-dependent photoluminescence," *Submitted to ACS Applied Materials & Interfaces*, vol. Under Review, no. Manuscript ID: am-2020-208267.

[18] R. Ma *et al.*, "Establishing Multifunctional Interface Layer of Perovskite Ligand Modified Lead Sulfide Quantum Dots for Improving the Performance and Stability of Perovskite Solar Cells," *Small*, vol. 16, no. 41, p. 2002628, 2020, doi: 10.1002/smll.202002628.

[19] J. Shi *et al.*, "Eliminating the electric field response in a perovskite heterojunction solar cell to improve operational stability," *Science Bulletin*, vol. 66, no. 6, pp. 536–544, Mar. 2021, doi: 10.1016/j.scib.2020.11.004.

[20] K. Domanski *et al.*, "Migration of cations induces reversible performance losses over day/night cycling in perovskite solar cells," *Energy & Environmental Science*, vol. 10, no. 2, pp. 604–613, 2017, doi: 10.1039/C6EE03352K.

[21] S. Kim *et al.*, "Relationship between ion migration and interfacial degradation of CH3NH3PbI3 perovskite solar cells under thermal conditions," *Sci Rep*, vol. 7, no. 1, p. 1200, Apr. 2017, doi: 10.1038/s41598-017-00866-6.

[22] J. Han *et al.*, "Hybrid PbS Quantum-Dot-in-Perovskite for High-Efficiency Perovskite Solar Cell," *Small*, vol. 14, no. 31, p. 1801016, 2018, doi: 10.1002/smll.201801016.

[23] Y. Yang *et al.*, "Novel Hybrid Ligands for Passivating PbS Colloidal Quantum Dots to Enhance the Performance of Solar Cells," *Nano-Micro Lett.*, vol. 7, no. 4, pp. 325–331, Oct. 2015, doi: 10.1007/s40820-015-0046-4.

[24] R. W. Crisp *et al.*, "Metal halide solid-state surface treatment for high efficiency PbS and PbSe QD solar cells," *Sci Rep*, vol. 5, p. 9945, Apr. 2015, doi: 10.1038/srep09945.

[25] X. Zhang *et al.*, "Inorganic CsPbI3 Perovskite Coating on PbS Quantum Dot for Highly Efficient and Stable Infrared Light Converting Solar Cells," *Advanced Energy Materials*, vol. 8, no. 6, p. 1702049, 2018, doi: 10.1002/aenm.201702049.